Neuron
Report

Norepinephrine Controls Astroglial Responsiveness to Local Circuit Activity

Martin Paukert,[1,4,5,*] Amit Agarwal,[1,4] Jaepyeong Cha,[2] Van A. Doze,[3] Jin U. Kang,[2] and Dwight E. Bergles[1,*]
[1]Solomon H. Snyder Department of Neuroscience, Johns Hopkins University School of Medicine, 725 N. Wolfe Street, WBSB 1001, Baltimore, MD 21205, USA
[2]Department of Electrical and Computer Engineering, Johns Hopkins University, 3400 N. Charles Street, Baltimore, MD 21218, USA
[3]Department of Basic Sciences, School of Medicine and Health Sciences, University of North Dakota, 501 N. Columbia Road Stop 9061, Grand Forks, ND 58202, USA
[4]Co-first author
[5]Present address: Department of Physiology, University of Texas Health Science Center at San Antonio, 8403 Floyd Curl Drive, STRF 208.2, San Antonio, TX 78229, USA
*Correspondence: paukertm@uthscsa.edu (M.P.), dbergles@jhmi.edu (D.E.B.)
http://dx.doi.org/10.1016/j.neuron.2014.04.038

SUMMARY

Astrocytes perform crucial supportive functions, including neurotransmitter clearance, ion buffering, and metabolite delivery. They can also influence blood flow and neuronal activity by releasing gliotransmitters in response to intracellular Ca^{2+} transients. However, little is known about how astrocytes are engaged during different behaviors in vivo. Here we demonstrate that norepinephrine primes astrocytes to detect changes in cortical network activity. We show in mice that locomotion triggers simultaneous activation of astrocyte networks in multiple brain regions. This global stimulation of astrocytes was inhibited by alpha-adrenoceptor antagonists and abolished by depletion of norepinephrine from the brain. Although astrocytes in visual cortex of awake mice were rarely engaged when neurons were activated by light stimulation alone, pairing norepinephrine release with light stimulation markedly enhanced astrocyte Ca^{2+} signaling. Our findings indicate that norepinephrine shifts the gain of astrocyte networks according to behavioral state, enabling astrocytes to respond to local changes in neuronal activity.

INTRODUCTION

Astrocytes are an essential component of neural circuits in vivo. They form highly interconnected networks, in which individuals occupy distinct domains that are extensively coupled through gap junctions. Each cell extends highly ramified processes that ensheath synapses, make contact with nodes of Ranvier, and form endfeet specializations on blood vessels, placing these cells in an ideal position to both control the extracellular milieu and influence neuronal activity. Indeed, astrocytes have been shown to participate in diverse functions, including neurotransmitter clearance, ion homeostasis (Djukic et al., 2007), hemodynamic control (Mulligan and MacVicar, 2004), and synaptic plasticity (Min and Nevian, 2012). However, there is still uncertainty about how astrocyte networks are controlled in vivo and when they engage in these distinct behaviors.

Astrocytes express an extensive complement of Gq-coupled neurotransmitter receptors that liberate Ca^{2+} from intracellular stores, providing a means to adjust their behavior in response to changes in neural activity. Ca^{2+} signaling in astrocytes has been linked to diverse phenomena, including changes in blood vessel diameter (Attwell et al., 2010; Mulligan and MacVicar, 2004) and synaptic plasticity (Di Castro et al., 2011; Min and Nevian, 2012; Jourdain et al., 2007), suggesting that the impact of astrocytes on various aspects of brain physiology is controlled by these metabotropic receptors. Nevertheless, the role of Ca^{2+} signaling in astrocytes in vivo remains uncertain, and mice that lack IP3R2 Ca^{2+} release channels that are responsible for receptor-evoked Ca^{2+} transients are overtly normal (Petravicz et al., 2008). Our lack of understanding about the interaction of astrocytes with neural circuits reflects our limited knowledge about the behavioral contexts in which astrocyte networks are activated. Despite evidence that astrocytes are responsive to multiple neurotransmitters, the pathways used to activate astrocytes in vivo and the patterns of activity that they exhibit during different behaviors remain to be defined.

In vivo two-photon imaging using Ca^{2+}-sensitive dyes has revealed that astrocyte network activity can be enhanced by local glutamatergic signaling (Nimmerjahn et al., 2009; Schummers et al., 2008) or by stimulation of long-range cholinergic (Takata et al., 2011; Chen et al., 2012) or noradrenergic (Bekar et al., 2008; Ding et al., 2013) neuromodulatory projections. How these local and global neuronal pathways interact to control the activity of astrocyte networks in awake, behaving animals has not been determined. Here we developed mice that express the genetically encoded Ca^{2+} indicator GCaMP3 in astrocytes and used in vivo two-photon imaging to define the activity patterns of cortical and cerebellar astrocytes during locomotion. Our results indicate that the increase in arousal that accompanies locomotion promotes widespread activation of astrocyte networks in the cortex and enhances their responsiveness to local changes in neuronal activity.

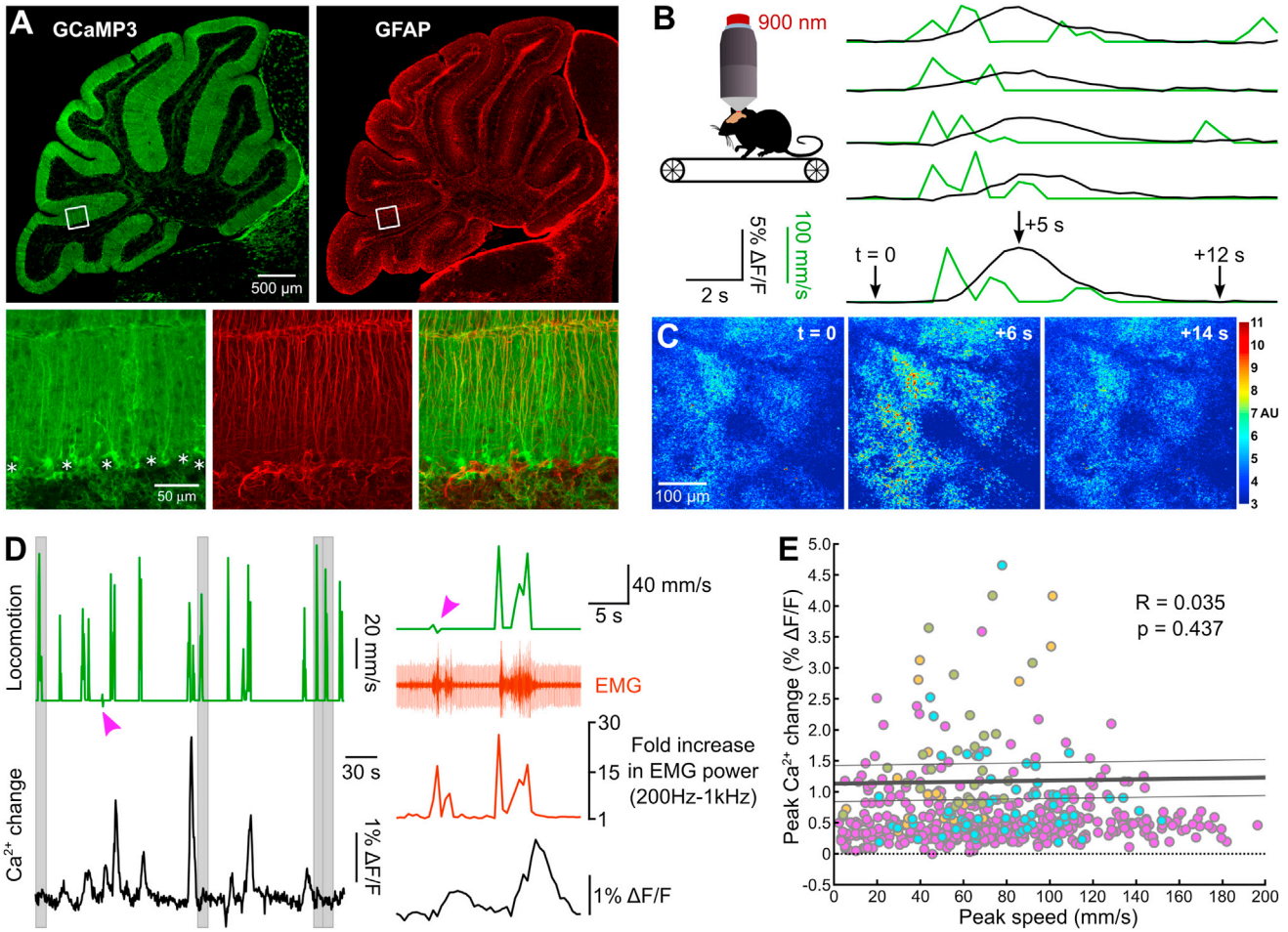

Figure 1. Weak Correlation between Voluntary Locomotion and Ca^{2+} Elevation in Bergmann Glia

(A) Cerebellar section from a 5-week-old *GLAST-CreER;R26-lsl-GCaMP3* mouse immunostained for GCaMP3 and glial fibrillary acidic protein (GFAP). Boxed areas are shown at higher magnification below. Asterisks highlight Purkinje cell somata devoid of fluorescence. (B) Left: schematic of imaging configuration. Right: five representative trials showing Bergmann glia Ca^{2+} increase (GCaMP3 fluorescence, black traces) relative to mouse locomotion (optical encoder, green traces). (C) Images of GCaMP3 fluorescence in Bergmann glial processes at times indicated by arrows in (B). (D) Left: continuous record of locomotion (green trace) and Bergmann glia Ca^{2+} levels (black trace, GCaMP3 fluorescence). Gray bars highlight periods when locomotion was not associated with Bergmann glia Ca^{2+} elevations. Arrowhead highlights a Bergmann glia Ca^{2+} transient that was not associated with locomotion. Right: expanded portion of trial including electromyography (EMG) signal. Arrowhead indicates timing of Bergmann glia Ca^{2+} elevation. (E) Plot of locomotion speed and Bergmann glia Ca^{2+} change (GCaMP3 fluorescence) for 707 locomotion periods from 4 mice. Colors represent trials from different individuals. Black lines represent mean ± SEM of 4 regression lines.

RESULTS

Ca^{2+} Transients in Bergmann Glia during Locomotion Depend on Animal State of Arousal

To define the mechanisms that control astrocyte activity in vivo, we developed transgenic knockin mice (*R26-lsl-GCaMP3*) in which the genetically encoded Ca^{2+} indicator GCaMP3 can be expressed in a cell-specific manner (Figure S1 available online). After breeding to *GLAST-CreER* mice, tamoxifen administration induced GCaMP3 expression in 35% ± 2% of cortical astrocytes (n = 20 mice) (Figure S1C) and 100% of Bergmann glia (n = 17 mice), a distinct group of astroglial cells found in the cerebellar cortex (Figure 1A; Figure S1C), which could be visualized in vivo for weeks to months using two-photon imaging through a cranial window (Movie S1). Apart from neurons (dentate gyrus granule cells, olfactory bulb interneurons) derived from SVZ/SGZ progenitors that express GLAST, no neuronal expression was detected in these mice.

Locomotion has been shown to trigger a transient rise in intracellular Ca^{2+} in Bergmann glia (Nimmerjahn et al., 2009). This activity, visualized acutely with a Ca^{2+} indicator dye, extended over large areas of the cerebellum and required local activation of glutamate receptors. To define the mechanisms required to engage this glial network, we trained GCaMP3-expressing mice to walk on a treadmill and monitored locomotion-induced Ca^{2+} levels in Bergmann glia. In accordance with previous findings (Nimmerjahn et al., 2009), brief bouts of locomotion were often associated with widespread elevation of Ca^{2+} in Bergmann glia that persisted for many seconds after cessation of movement (Figure 1B; Movie S2). However, the magnitude of the

Bergmann glia Ca^{2+} response was not correlated with locomotion speed (R = 0.0352, p = 0.4365, 495 events from 4 mice), and locomotion often did not trigger activation of Bergmann glia (212 failures in 707 locomotion events). As comparable bouts of locomotion should produce similar activity in glutamatergic afferents, these results suggest that other signaling pathways are involved in recruitment of these glial cells. Indeed, Bergmann glia often exhibited widespread activity in the absence of locomotion (Figures 1D and 1E) (83 events, 4 mice).

To provide an independent measure of motor activity in these mice, we monitored muscle contraction during imaging trials. Post hoc analysis of electromyogram (EMG) recordings revealed that "spontaneous" Ca^{2+} transients that occurred in the absence of locomotion were often associated with an increase in EMG power (73/83 events, 3 mice), suggestive of startle behavior. This observation raised the possibility that activity in Bergmann glia may correspond to an increase in arousal. To facilitate pharmacological analysis of locomotion-induced Bergmann glial Ca^{2+} responses, we standardized their motor activity by subjecting mice to brief periods (5 s) of forced locomotion. Strikingly, enforced locomotion consistently evoked large Ca^{2+} transients throughout the Bergmann glia network (Figure 2A). Ca^{2+} transients induced by enforced locomotion had a similar time course to events that occurred during voluntary locomotion (enforced: half-maximum width, 8.30 ± 0.60 s, n = 159 events; voluntary: 8.26 ± 1.24 s, n = 13 events, 5 mice, p = 0.975) (Figure 2B) and enforced events that immediately followed voluntary events were depressed by 47% ± 5% (n = 11 events, 7 mice, $p < 0.001$) (Figure 2C), suggesting that similar pathways are activated during both voluntary and enforced locomotion.

Norepinephrine Induces Ca^{2+} Elevations in Bergmann Glia during Locomotion

We assessed whether antagonists of different neuromodulatory receptors attenuated Bergmann glia Ca^{2+} changes induced by locomotion. Although Bergmann glia responses were not affected by peripheral administration of CNS accessible antagonists of serotonergic, muscarinic, metabotropic glutamate, or cannabinoid receptors, administration of trazodone, a broad-spectrum inhibitor of adrenergic, serotonergic, and histaminergic receptors (Cusack et al., 1994), dramatically reduced locomotion-induced Ca^{2+} transients in these cells without altering the intensity of their motor response (EMGs) (Figures 2D–2F). Increases in arousal are often associated with the release of norepinephrine (Foote et al., 1980), raising the possibility that the trazodone-induced block of Ca^{2+} signaling in Bergmann glia is due to an inhibition of the noradrenergic signaling. Indeed, chemical depletion of norepinephrine with the neurotoxin DSP4 (Jonsson et al., 1981) abolished Bergmann glia Ca^{2+} transients induced by either voluntary or enforced locomotion (Figure S2), indicating that norepinephrine plays a key role in activating these astroglial cells during this behavior. The histaminergic H1 receptor antagonist diphenhydramine (DPH) also partially inhibited Bergmann glia responses, possibly due to its antagonism at α1-adrenoceptors (Kester et al., 2003). To define the receptor subtypes responsible, we locally applied selective adrenoceptor antagonists to the cerebellar surface between imaging sessions. Locomotion-induced Ca^{2+} transients were strongly inhibited by the α1-adrenergic receptor antagonist terazosin but not by the β-adrenoceptor antagonist metoprolol (Figure 2G). In contrast, AMPA and NMDA receptor antagonists attenuated but did not block this activity, suggesting that local glutamatergic and noradrenergic signaling act synergistically in the cerebellar cortex to promote Bergmann glia activity.

Locomotion-Induced Norepinephrine Release Activates Astrocytes in Visual Cortex

Noradrenergic neurons in the brainstem nucleus locus coeruleus (LC) extend axon collaterals diffusely throughout the brain, providing the means to exert control over brain activity states (Steindler, 1981). To determine whether locomotion-induced engagement of the noradrenergic system results in global activation of astrocytes throughout the brain, we monitored astrocyte Ca^{2+} levels in primary visual cortex (V1) during locomotion (Figures 3A–3C). Remarkably, in complete darkness, enforced locomotion reliably elicited Ca^{2+} transients in V1 astrocytes that had a similar time course to Bergmann glia responses in the cerebellum (Figures 3D and 3E; Movie S3). Locomotion-induced astrocyte activity in V1 was similarly blocked by trazodone and abolished by depletion of norepinephrine with DSP4 (Figure S3). To assess the relative timing and spatial extent of changes in astrocyte activity, we developed a dual fiber-optic imaging system to monitor GCaMP3 fluorescence simultaneously in different brain regions (Figure 3F). When fiber-optic probes were positioned over cranial windows implanted above the visual cortex (V1) and cerebellum (lobulus simplex), coincident Ca^{2+} elevations were detected in both astrocytes and Bergmann glia in response to voluntary and enforced locomotion (Figure 3G). The magnitude of Ca^{2+} changes in these two regions covaried (correlation coefficient = 0.756, $p < 0.001$; n = 348 events from 6 mice), suggesting that amplitude fluctuations arise primarily from different levels of activity in noradrenergic neurons. Although events in these regions began at the same time (cerebellum onset delay = 1.93 ± 0.13 s; V1 onset delay = 1.91 ± 0.10 s, 348 events from 6 mice, p = 0.8982), consistent with the minimal delay predicted to arise solely from differences in axonal length (~40 ms, assuming a conduction velocity of 0.5 m/s and an additional distance of 20 mm to V1), Ca^{2+} transients in visual cortex reached their peak 1.6 ± 0.2 s later than events in the cerebellum ($p < 0.001$), raising the possibility that local circuit activity modifies the timing of astrocyte recruitment.

Norepinephrine Enhances the Sensitivity of Astrocytes to Local Circuit Activity

Locomotion induces release of norepinephrine in the visual cortex in complete darkness, providing a means to determine whether activation of this endogenous neuromodulatory input influences the response of astrocytes to local network activity. To assess the effects of norepinephrine, we monitored the behavior of groups of V1 astrocytes to locomotion, light stimulation alone, and locomotion paired with light stimulation. Enforced locomotion reliably elicited Ca^{2+} transients in V1 astrocytes, although the response of individual cells was variable, with some cells responding to each trial and others responding to only a subset of trials (Figures 4A and 4B). In contrast, light stimulation alone rarely activated V1 astrocytes, despite triggering large evoked

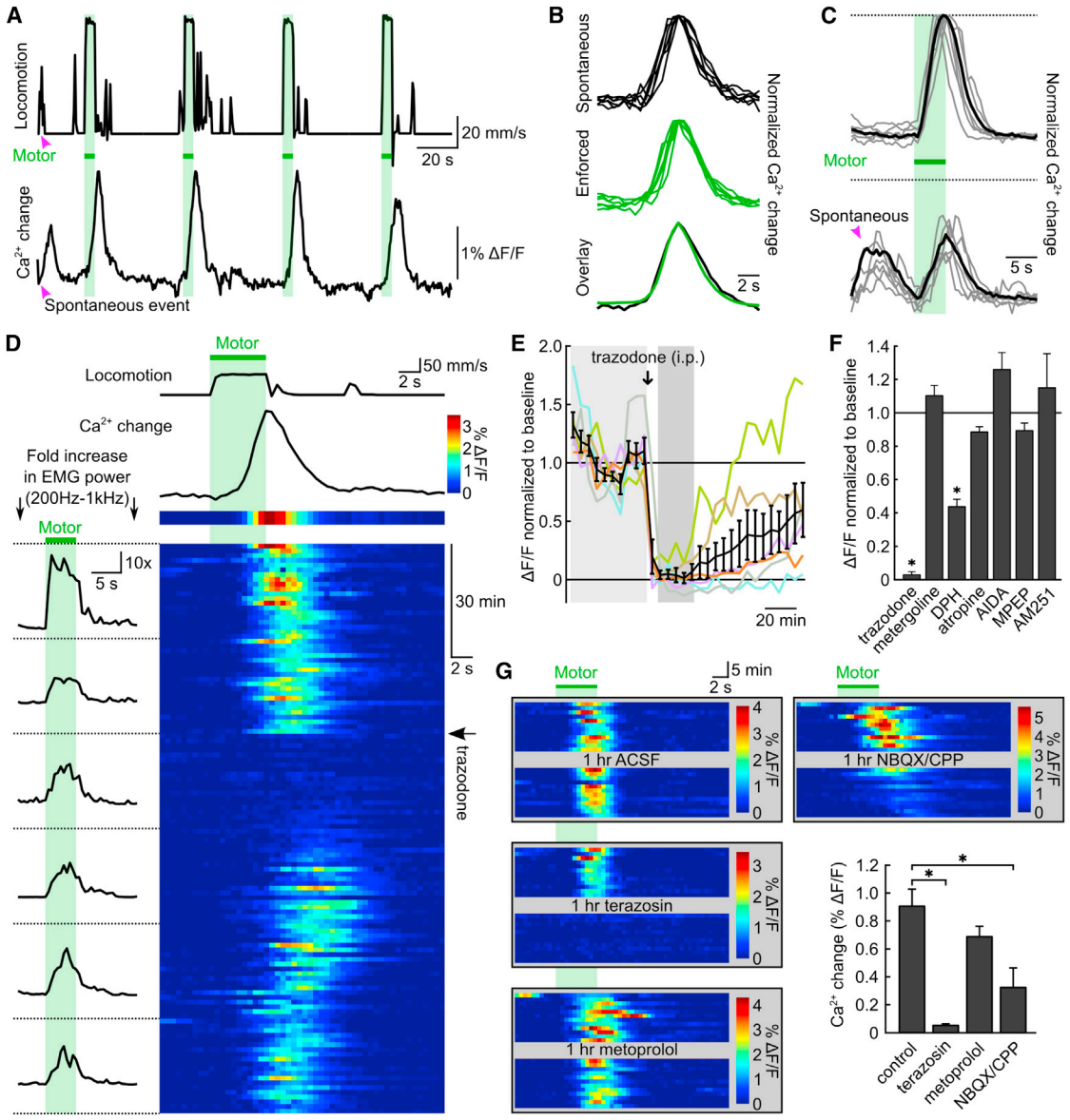

Figure 2. Noradrenergic Signaling Is Required for Locomotion-Induced Activation of Bergmann Glia

(A) Spontaneous (arrowhead) and enforced (green bars) locomotion and corresponding Bergmann glia Ca^{2+} levels (GCaMP3 fluorescence). (B) Normalized Bergmann glia Ca^{2+} changes associated with spontaneous (6 of 13 events) and enforced locomotion (6 of 159 events) from experiment in (A). (C) Individual (gray traces) and average (black traces) Bergmann glia Ca^{2+} transients resulting from enforced locomotion with (bottom traces) or without (top traces) a preceding spontaneous event. (D) Consecutive trials of enforced locomotion (green bar) pseudocolored according to magnitude of Ca^{2+} change. Arrow indicates time of trazodone injection (10 mg/kg i.p.). Left: average EMG power during 20 consecutive trials at right. (E) Normalized amplitude of Bergmann glia Ca^{2+} elevations elicited by enforced locomotion. Each point is average of four consecutive trials normalized to baseline. Regions highlighted by light gray bar used to determine baseline and dark gray bar the maximal response to drug. Black symbols represent mean ± SEM. (F) Effect of neuromodulatory receptor antagonists on Bergmann glia Ca^{2+} response to enforced locomotion. Columns represent mean ± SEM. Concentrations from left: 10, 10, 20, 20, 20, 20, and 10 mg/kg i.p. Number of experiments from left: 6, 5, 5, 5, 5, 4, and 3. Asterisks indicate significant reduction relative to baseline in one-way ANOVA followed by Bonferroni post hoc test. (G) Bergmann glia Ca^{2+} transients in consecutive trials of enforced locomotion before and after local application of antagonists. Summary graph represents mean ± SEM. Concentrations are the following: 100 μM terazosin, 3 μM metoprolol, 300/200 μM NBQX/CPP. Number of experiments from left: 8, 5, 5, and 5. Asterisks indicate significant difference in one-way ANOVA followed by Bonferroni post hoc test.

potentials and inducing hemodynamic changes in this area (Figures S4A and S4B). Occasional coincident astrocyte activity that occurred in response to light stimulation was always associated with enhanced EMG power (Figure 4A), reflecting voluntary locomotion of the animals or possible startle behavior. Despite the weak activation of V1 astrocytes by visual input, pairing locomotion with light stimulation markedly enhanced astrocyte activity above that produced by locomotion alone, without altering

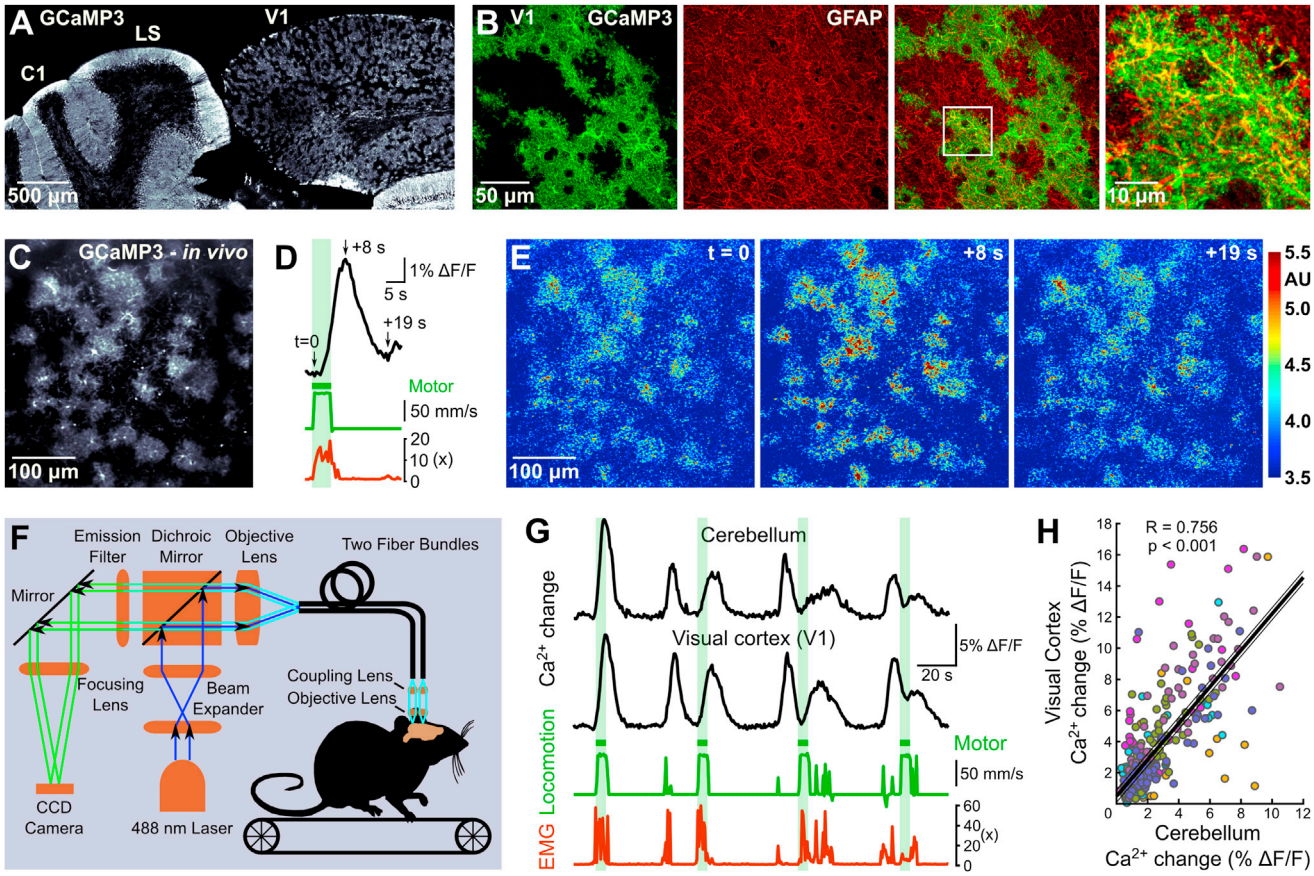

Figure 3. Locomotion Induces Simultaneous Activation of Astroglia in Different Regions of the Brain

(A) Parasagittal section of *GLAST-CreER;R26-lsl-GCaMP3* mouse (P57) immunostained for GCaMP3. C1, crus1; LS, lobulus simplex; V1, primary visual cortex. (B) Higher-magnification image of GCaMP3 (green) and GFAP (red) in V1. (C) In vivo image of V1, layer 1 (70 µm below pial surface) cortical astrocytes expressing GCaMP3 in 3-month-old *GLAST-CreER;R26-lsl-GCaMP3* mouse. (D) Mean change in cytosolic Ca^{2+} (GCaMP3) in V1 cortical astrocytes (black trace) induced by enforced locomotion (green trace). Green bar: period of enforced locomotion; green trace: locomotion; red trace: fold increase in EMG activity. (E) Images of GCaMP3 fluorescence in V1 astrocytes at times indicated in (D). (F) Schematic of dual fiber-optic photometry configuration. (G) Ca^{2+} changes in Bergmann glia and V1 astrocytes visualized simultaneously during enforced locomotion (green bars) and corresponding EMG activity. (H) Covariance between Bergmann glia and V1 astrocyte Ca^{2+} changes during spontaneous locomotion. n = 348 spontaneous locomotion events from 6 mice. Black lines represent mean ± SEM of 6 regression lines.

motor output as measured by EMG (Figures 4A–4D). Analysis of individual astrocytes revealed that light stimulation increased both the amplitude of Ca^{2+} transients in each cell and the proportion of cells that responded to each trial (Figures 4B and 4C). To assess whether the highly ramified processes of astrocytes, which are comprised of distinct microdomains (Grosche et al., 1999), exhibit Ca^{2+} transients with thresholds and kinetics distinct from those observed at the soma, we analyzed Ca^{2+} events in astrocyte processes and somata independently by masking individual astrocyte somata within the field; these non-somatic regions yielded signals from both the main processes and the highly ramified segments within the neuropil. Although it is possible that some microdomain activity may go undetected using our imaging method, astrocyte processes responded very similarly to their somata (Figures S4C–S4H), suggesting that α1 adrenoceptors are widely distributed in astrocyte membranes.

DISCUSSION

These findings indicate that astrocytes throughout the brain are activated by norepinephrine during periods of heightened vigilance and that this modulation plays a critical role in enabling these glial cells to respond to local network activity. Unlike fast excitatory and inhibitory neurotransmitters, where transmission occurs at synapses defined by directly apposed pre- and postsynaptic elements, norepinephrine is released from axonal varicosities into the surrounding neuropil, a "volume transmission" that enables multiple targets in the surrounding area to be affected. Astroglia appear to be a direct target of the noradrenergic system, as gene expression profiling indicates that they express a variety of Gq-coupled alpha adrenergic receptors (Cahoy et al., 2008); exogenous norepinephrine triggers a rise in Ca^{2+} in cultured astrocytes (Salm and McCarthy, 1990) as well as astrocytes and Bergmann glia in acute brain slices

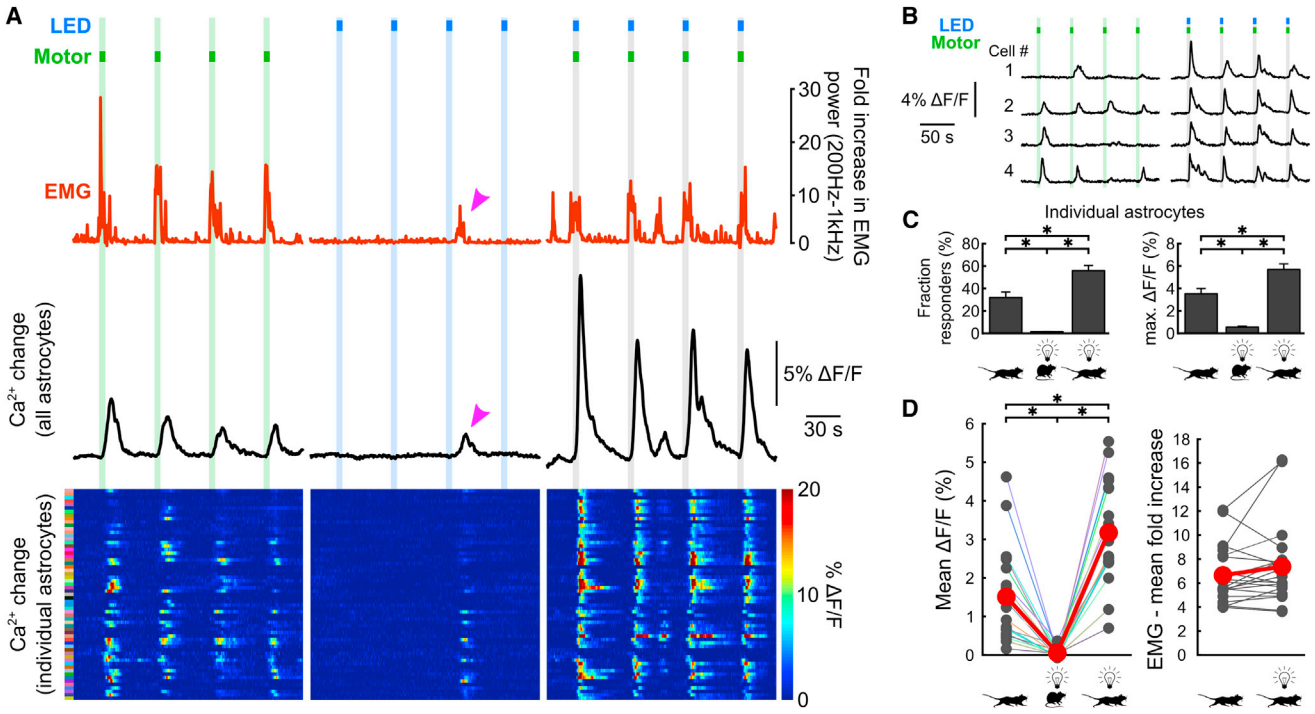

Figure 4. Norepinephrine Enhances the Sensitivity of Astrocytes to Local Circuit Activity

(A) V1 astrocyte Ca^{2+} responses to enforced locomotion (green bars), visual stimulation (blue bars), or simultaneous enforced locomotion and visual stimulation (gray bars). Red traces represent EMG activity; black traces represent mean Ca^{2+} change in all astrocytes. Bottom: Ca^{2+} changes in individual astrocytes pseudocolored according to amplitude. Arrowhead highlights Ca^{2+} elevation associated with spontaneous locomotion. (B) Ca^{2+} transients in four representative cells during four consecutive trials of enforced locomotion (green bars) or simultaneous enforced locomotion and visual stimulation (gray bars). (C) Left: average fraction of astrocytes responding with a mean Ca^{2+} elevation exceeding 1% ΔF/F. Right, average maximum Ca^{2+} responses in individual astrocytes (16–20 trials). Error bars represent mean ± SEM; n = 20 mice; asterisks indicate significant difference (one-way ANOVA with Bonferroni post hoc test). (D) Left: mean Ca^{2+} elevations in all astrocytes (16–20 trials). Colored lines connect data points from individual mice. Asterisks indicate significant difference (one-way ANOVA with Bonferroni post hoc test). Right: change in EMG power during enforced locomotion or simultaneous enforced locomotion and visual stimulation. Each point represents average response in 16–20 trials. Red circles indicate mean of all trials.

when neuronal activity is blocked (Duffy and MacVicar, 1995; Shao and McCarthy, 1997), and aversive stimuli or direct electrical stimulation of the LC induces Ca^{2+} transients in astrocytes in the somatosensory cortex (Bekar et al., 2008; Ding et al., 2013). The mechanisms that enhance the responsiveness of astrocytes to local increases in neuronal activity are unknown but may involve intracellular changes in signaling intermediates that enhance the ability of other Gq-coupled metabotropic receptors to induce Ca^{2+} release from intracellular stores (Ryzhov et al., 2006). It is also possible that synergy occurs by enhancing the release of norepinephrine in V1, leading to larger, more prolonged Ca^{2+} transients in astrocytes. This effect could be initiated locally in the cortex or by enhancing the activity of these neurons at the level of the LC. Direct assessment of the activity of noradrenergic projections to V1 during this behavior would help to define whether their activity is modulated in this form of plasticity.

Reduced Responsiveness of Astrocyte Networks in Unanesthetized Mice

The close association of astrocytes with synapses allows detection of neuronal activity and the potential for feedback modulation (Parpura et al., 1994; Di Castro et al., 2011; Jourdain et al., 2007; Saab et al., 2012). Thus, it was unexpected that exposure to strong visual stimulation alone failed to engage astrocyte networks in V1, particularly given previous studies demonstrating robust activation of V1 astrocytes with light in anesthetized mice (Chen et al., 2012). However, anesthesia has been shown to dramatically expand active regions in mouse V1 and prolong responses to visual stimulation (Haider et al., 2013), which may lower the threshold for astrocyte activation. Moreover, astrocytes have been implicated in the regulation of sleep-wake cycles (Halassa et al., 2009) and their functional state differs considerably between sleep/anesthesia and wakefulness (Xie et al., 2013). It has also been reported that astrocyte Ca^{2+} signaling in vivo is inhibited by various anesthetics (Nimmerjahn et al., 2009; Thrane et al., 2012), raising concern that the depth of anesthesia and type of anesthetic can dramatically alter their responsiveness. Together, these findings highlight the importance of defining astrocyte activity in awake animals during different behavioral states.

Norepinephrine Enhances the Gain of Both Astrocyte and Neuronal Networks

These studies indicate that astrocyte networks have a high threshold for activation in periods of quiescence and suggest

that recruitment of the noradrenergic system is required to enhance the gain of these networks to enable local interactions between astrocytes and neurons in circuits involved in processing sensory information. The activation of astrocytes in V1 by norepinephrine during locomotion parallels recent in vivo electrophysiological studies indicating that locomotion triggers norepinephrine-dependent depolarization of neurons in V1 (Polack et al., 2013). In contrast to neuronal activation, which began within 50 ms of locomotion onset, Ca^{2+} transients in astrocytes began more than a second later (1.4 ± 0.1 s, n = 106 events from 13 mice), presumably reflecting the additional biochemical steps required to release Ca^{2+} from intracellular stores. These results suggest that astrocyte Ca^{2+} transients are unlikely to be causal for the initial depolarization of cortical neurons, for example, by stimulating the release of gliotransmitters; however, Ca^{2+} is not the only signaling intermediate produced by activation of α adrenoceptors and astrocytes may express adrenoceptors coupled to other G proteins (e.g., Gi) (Cahoy et al., 2008) that could trigger responses on a timescale coincident with neuronal depolarization. The ability of astroglia to detect the coincidence of arousal and local network activity may allow these cells to contribute to sensory-specific attentional shifts (Cohen and Maunsell, 2011), promoted by the slow onset and prolonged nature of their Ca^{2+} responses. Future analysis of mice in which alpha adrenoceptors have been selectively removed from astrocytes will help to define their role in noradrenergic modulation of cortical networks and arousal states.

Astrocytes are well positioned to amplify the effects of diffuse neuromodulatory projections; their highly ramified processes not only increase the probability of interaction with low concentrations of neurotransmitters but also shield neurons by increasing the diffusional distance from varicosities to neuronal membranes. Although the exact complement of neurotransmitter receptors expressed by astrocytes in different brain regions has not been defined, cortical astrocytes have also been shown to respond to glutamate, ATP, and acetylcholine (Verkhratsky and Kettenmann, 1996; Takata et al., 2011). The ability to stably express Ca^{2+} indicators selectively in astrocytes in vivo using conditional GCaMP3 mice and viral-based delivery methods (Shigetomi et al., 2013) will help define the behavioral contexts in which these different receptors become activated and reveal how they influence interactions between neurons and astrocytes in distinct neural circuits.

EXPERIMENTAL PROCEDURES

Animals

Cre recombinase-conditional GCaMP3 mice were generated using a knockin strategy into the ROSA26 locus and crossed to *GLAST-CreER* mice to enable GCaMP3 expression in astrocytes and Bergmann glia. Cranial windows were implanted above the cerebellum or V1.

In Vivo Two-Photon Imaging

Fluorescence images were collected using a Movable Objective Microscope (MOM) (Sutter Instruments) with a 20×, 1.0 NA objective (Zeiss). Image acquisition rate was 2 frames/s.

Dual Optic Fiber Bundle Imaging

For simultaneous imaging of astroglial Ca^{2+} changes in cerebellum and visual cortex, cranial windows were implanted and two multicore optical fibers aligned above these regions. The light path is illustrated in Figure 3F. No optical crosstalk between fiber bundles was detected: the objective lens pairs had a diameter of 2.4 mm and a working distance of 0.88 mm.

Locomotion Behavioral Paradigm

Mice were placed on a custom-designed linear treadmill and their heads immobilized. The treadmill was either freely movable or placed under motor control and the motion of the treadmill belt was monitored with an optical encoder.

Electromyography

Body surface potentials were recorded as the voltage between two silver wires placed subcutaneously at the right shoulder and left hip.

Visual Stimulation

A UV-LED with a Lambertian emission profile was used as a light source at a distance of 40 mm, centered between the eyes to achieve uniform light exposure.

Data Analysis

Data were processed and analyzed in MATLAB. ΔF/F fluorescence intensity traces represent $(F - F_{median})/F_{median}$, with F representing mean fluorescence value of all pixels within a region of interest (ROI) of one image frame and F_{median} representing median F of all image frames.

Statistical Analysis

The following statistical analyses were used: Figures 1E and 3H, analysis of covariance for correlation within subjects; Figures 2B, 2C, and 4D (right), difference in onset of response in Figures 3F–3H, Figures S2 and S3, one-tailed paired t test; Figures 2F, 2G, 4C, and 4D (left), one-way ANOVA followed by Bonferroni post hoc test; text, difference in peak of response in Figures 3F–3H, one-sample t test.

Additional information about the procedures used in this study is described in the Supplemental Experimental Procedures.

SUPPLEMENTAL INFORMATION

Supplemental Information includes Supplemental Experimental Procedures, four figures, and three movies and can be found with this article online at http://dx.doi.org/10.1016/j.neuron.2014.04.038.

AUTHOR CONTRIBUTIONS

M.P., A.A., and D.E.B. conceived the project. M.P. and D.E.B. designed the experiments and wrote the manuscript with help from the other authors. M.P. conducted experiments, developed software, and analyzed data. A.A. generated and characterized the *R26-lsl-GCaMP3* mice, J.C. and J.K. developed the dual fiber imaging probe and assisted with fiber-optic imaging, and V.A.D. provided assistance with adrenergic receptor pharmacology.

ACKNOWLEDGMENTS

We thank L. Looger for providing the GCaMP3 construct, J. Nathans for providing *GLAST-CreER* mice and assistance with Rosa26 targeting, M. Fukaya for providing antibodies, Terry Shelley for his machining expertise, and Naiqing Ye for assistance with animal colony maintenance. This work was supported by grants from the NIAAA (AA022239) to M.P., the NIMH (Conte Center for Neuroscience, MH084020), the Brain Science Institute and the Science of Learning Institute at Johns Hopkins to D.E.B. A.A. was supported by a postdoctoral fellowship from the National Multiple Sclerosis Society.

Accepted: April 11, 2014
Published: June 18, 2014

REFERENCES

Attwell, D., Buchan, A.M., Charpak, S., Lauritzen, M., Macvicar, B.A., and Newman, E.A. (2010). Glial and neuronal control of brain blood flow. Nature *468*, 232–243.

Bekar, L.K., He, W., and Nedergaard, M. (2008). Locus coeruleus alpha-adrenergic-mediated activation of cortical astrocytes in vivo. Cereb. Cortex *18*, 2789–2795.

Cahoy, J.D., Emery, B., Kaushal, A., Foo, L.C., Zamanian, J.L., Christopherson, K.S., Xing, Y., Lubischer, J.L., Krieg, P.A., Krupenko, S.A., et al. (2008). A transcriptome database for astrocytes, neurons, and oligodendrocytes: a new resource for understanding brain development and function. J. Neurosci. *28*, 264–278.

Chen, N., Sugihara, H., Sharma, J., Perea, G., Petravicz, J., Le, C., and Sur, M. (2012). Nucleus basalis-enabled stimulus-specific plasticity in the visual cortex is mediated by astrocytes. Proc. Natl. Acad. Sci. USA *109*, E2832–E2841.

Cohen, M.R., and Maunsell, J.H.R. (2011). Using neuronal populations to study the mechanisms underlying spatial and feature attention. Neuron *70*, 1192–1204.

Cusack, B., Nelson, A., and Richelson, E. (1994). Binding of antidepressants to human brain receptors: focus on newer generation compounds. Psychopharmacology (Berl.) *114*, 559–565.

Di Castro, M.A., Chuquet, J., Liaudet, N., Bhaukaurally, K., Santello, M., Bouvier, D., Tiret, P., and Volterra, A. (2011). Local Ca2+ detection and modulation of synaptic release by astrocytes. Nat. Neurosci. *14*, 1276–1284.

Ding, F., O'Donnell, J., Thrane, A.S., Zeppenfeld, D., Kang, H., Xie, L., Wang, F., and Nedergaard, M. (2013). α1-Adrenergic receptors mediate coordinated Ca2+ signaling of cortical astrocytes in awake, behaving mice. Cell Calcium *54*, 387–394.

Djukic, B., Casper, K.B., Philpot, B.D., Chin, L.-S., and McCarthy, K.D. (2007). Conditional knock-out of Kir4.1 leads to glial membrane depolarization, inhibition of potassium and glutamate uptake, and enhanced short-term synaptic potentiation. J. Neurosci. *27*, 11354–11365.

Duffy, S., and MacVicar, B.A. (1995). Adrenergic calcium signaling in astrocyte networks within the hippocampal slice. J. Neurosci. *15*, 5535–5550.

Foote, S.L., Aston-Jones, G., and Bloom, F.E. (1980). Impulse activity of locus coeruleus neurons in awake rats and monkeys is a function of sensory stimulation and arousal. Proc. Natl. Acad. Sci. USA *77*, 3033–3037.

Grosche, J., Matyash, V., Möller, T., Verkhratsky, A., Reichenbach, A., and Kettenmann, H. (1999). Microdomains for neuron-glia interaction: parallel fiber signaling to Bergmann glial cells. Nat. Neurosci. *2*, 139–143.

Haider, B., Häusser, M., and Carandini, M. (2013). Inhibition dominates sensory responses in the awake cortex. Nature *493*, 97–100.

Halassa, M.M., Florian, C., Fellin, T., Munoz, J.R., Lee, S.-Y., Abel, T., Haydon, P.G., and Frank, M.G. (2009). Astrocytic modulation of sleep homeostasis and cognitive consequences of sleep loss. Neuron *61*, 213–219.

Jonsson, G., Hallman, H., Ponzio, F., and Ross, S. (1981). DSP4 (N-(2-chloroethyl)-N-ethyl-2-bromobenzylamine)—a useful denervation tool for central and peripheral noradrenaline neurons. Eur. J. Pharmacol. *72*, 173–188.

Jourdain, P., Bergersen, L.H., Bhaukaurally, K., Bezzi, P., Santello, M., Domercq, M., Matute, C., Tonello, F., Gundersen, V., and Volterra, A. (2007). Glutamate exocytosis from astrocytes controls synaptic strength. Nat. Neurosci. *10*, 331–339.

Kester, R.R., Mooppan, U.M., Gousse, A.E., Alver, J.E., Gintautas, J., Gulmi, F.A., Abadir, A.R., and Kim, H. (2003). Pharmacological characterization of isolated human prostate. J. Urol. *170*, 1032–1038.

Min, R., and Nevian, T. (2012). Astrocyte signaling controls spike timing-dependent depression at neocortical synapses. Nat. Neurosci. *15*, 746–753.

Mulligan, S.J., and MacVicar, B.A. (2004). Calcium transients in astrocyte endfeet cause cerebrovascular constrictions. Nature *431*, 195–199.

Nimmerjahn, A., Mukamel, E.A., and Schnitzer, M.J. (2009). Motor behavior activates Bergmann glial networks. Neuron *62*, 400–412.

Parpura, V., Basarsky, T.A., Liu, F., Jeftinija, K., Jeftinija, S., and Haydon, P.G. (1994). Glutamate-mediated astrocyte-neuron signalling. Nature *369*, 744–747.

Petravicz, J., Fiacco, T.A., and McCarthy, K.D. (2008). Loss of IP3 receptor-dependent Ca2+ increases in hippocampal astrocytes does not affect baseline CA1 pyramidal neuron synaptic activity. J. Neurosci. *28*, 4967–4973.

Polack, P.-O., Friedman, J., and Golshani, P. (2013). Cellular mechanisms of brain state-dependent gain modulation in visual cortex. Nat. Neurosci. *16*, 1331–1339.

Ryzhov, S., Goldstein, A.E., Biaggioni, I., and Feoktistov, I. (2006). Cross-talk between G(s)- and G(q)-coupled pathways in regulation of interleukin-4 by A(2B) adenosine receptors in human mast cells. Mol. Pharmacol. *70*, 727–735.

Saab, A.S., Neumeyer, A., Jahn, H.M., Cupido, A., Šimek, A.A.M., Boele, H.-J., Scheller, A., Le Meur, K., Götz, M., Monyer, H., et al. (2012). Bergmann glial AMPA receptors are required for fine motor coordination. Science *337*, 749–753.

Salm, A.K., and McCarthy, K.D. (1990). Norepinephrine-evoked calcium transients in cultured cerebral type 1 astroglia. Glia *3*, 529–538.

Schummers, J., Yu, H., and Sur, M. (2008). Tuned responses of astrocytes and their influence on hemodynamic signals in the visual cortex. Science *320*, 1638–1643.

Shao, Y., and McCarthy, K.D. (1997). Responses of Bergmann glia and granule neurons in situ to N-methyl-D-aspartate, norepinephrine, and high potassium. J. Neurochem. *68*, 2405–2411.

Shigetomi, E., Bushong, E.A., Haustein, M.D., Tong, X., Jackson-Weaver, O., Kracun, S., Xu, J., Sofroniew, M.V., Ellisman, M.H., and Khakh, B.S. (2013). Imaging calcium microdomains within entire astrocyte territories and endfeet with GCaMPs expressed using adeno-associated viruses. J. Gen. Physiol. *141*, 633–647.

Steindler, D.A. (1981). Locus coeruleus neurons have axons that branch to the forebrain and cerebellum. Brain Res. *223*, 367–373.

Takata, N., Mishima, T., Hisatsune, C., Nagai, T., Ebisui, E., Mikoshiba, K., and Hirase, H. (2011). Astrocyte calcium signaling transforms cholinergic modulation to cortical plasticity in vivo. J. Neurosci. *31*, 18155–18165.

Thrane, A.S., Rangroo Thrane, V., Zeppenfeld, D., Lou, N., Xu, Q., Nagelhus, E.A., and Nedergaard, M. (2012). General anesthesia selectively disrupts astrocyte calcium signaling in the awake mouse cortex. Proc. Natl. Acad. Sci. USA *109*, 18974–18979.

Verkhratsky, A., and Kettenmann, H. (1996). Calcium signalling in glial cells. Trends Neurosci. *19*, 346–352.

Xie, L., Kang, H., Xu, Q., Chen, M.J., Liao, Y., Thiyagarajan, M., O'Donnell, J., Christensen, D.J., Nicholson, C., Iliff, J.J., et al. (2013). Sleep drives metabolite clearance from the adult brain. Science *342*, 373–377.

Neuron, Volume *82*

Supplemental Information

Norepinephrine Controls Astroglial Responsiveness to Local Circuit Activity

Martin Paukert, Amit Agarwal, Jaepyeong Cha, Van A. Doze, Jin U. Kang, and Dwight E. Bergles

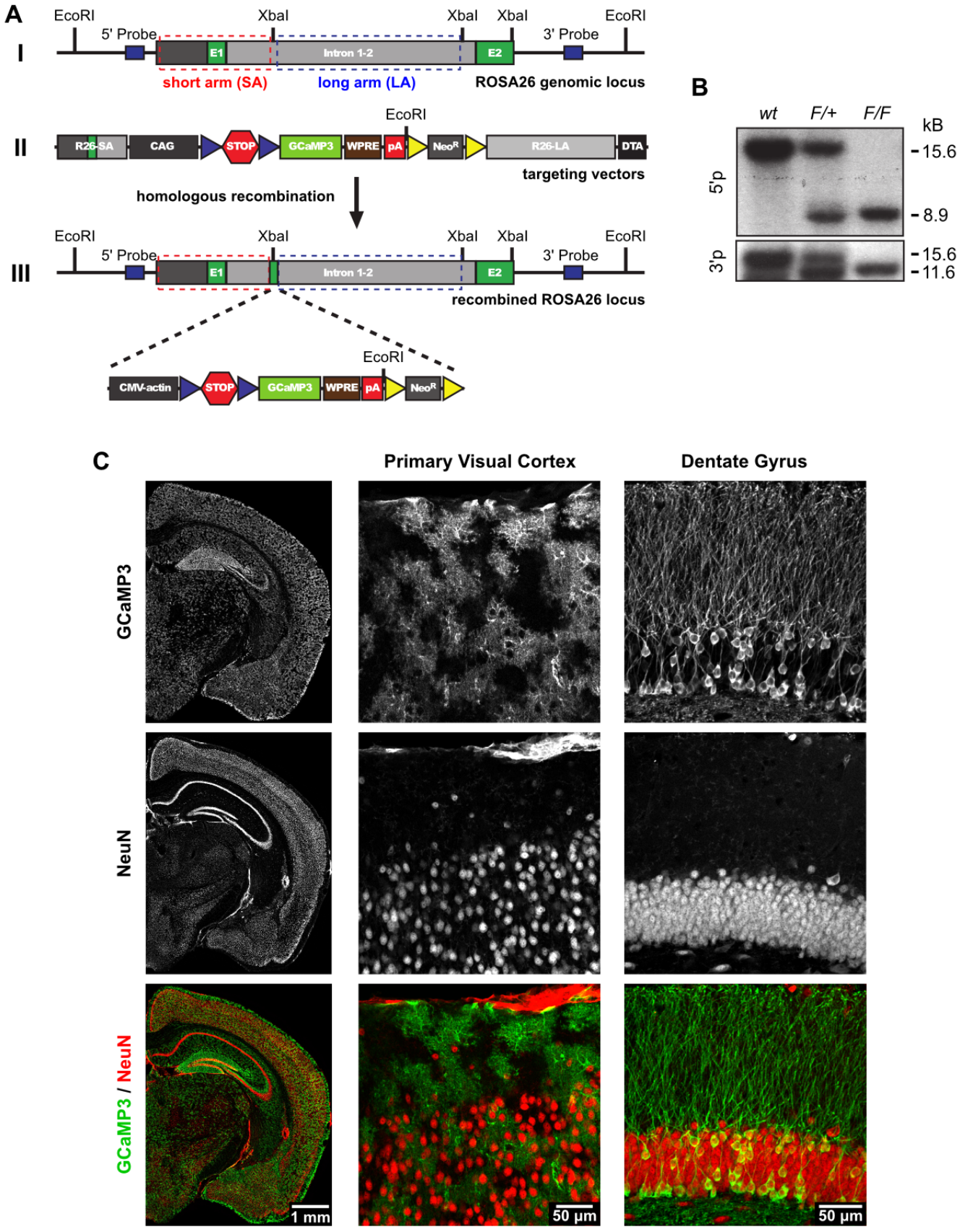
A
EcoRI
XbaI
XbaI
XbaI
EcoRI
5' Probe
3' Probe
I
E1
Intron 1-2
E2
short arm (SA)
long arm (LA)
ROSA26 genomic locus
EcoRI
II
R26-SA
CAG
STOP
GCaMP3
WPRE
pA
NeoR
R26-LA
DTA
targeting vectors
homologous recombination
EcoRI
XbaI
XbaI
XbaI
EcoRI
5' Probe
3' Probe
III
E1
Intron 1-2
E2
recombined ROSA26 locus
EcoRI
CMV-actin
STOP
GCaMP3
WPRE
pA
NeoR
B
wt
F/+
F/F
kB
5'p
3'p
15.6
8.9
15.6
11.6
C
Primary Visual Cortex
Dentate Gyrus
GCaMP3
NeuN
GCaMP3 / NeuN
1 mm
50 µm
50 µm

Figure S1

Figure S1 | Generation of conditional GCaMP3 transgenic mice, related to Figure 1. **A**, A gene trap strategy to 'knock in' GCaMP3 into the murine ROSA26 gene. (I) Genomic structure of the wildtype ROSA26 allele. The locus comprises two exons (E1 and E2; green boxes). The first XbaI restriction site located in intron 1-2 was used for gene trapping, mediated by homologous recombination in murine embryonic stem (ES) cells. (II) Structure of the GCaMP3 targeting vector. The construct harbors 5' (R26-SA) and 3' (R26-LA) homology arms from ROSA26, the CMV enhancer chicken β-actin hybrid (CAG) promoter (black box), loxP flanked 3x SV40-polyA "STOPPER" sequence (blue triangles and red hexagon), the GCaMP3 cDNA (light green box), Woodchuck post-transcriptional response element (WPRE, brown box), bovine growth hormone polyA sequence (pA, red box) and a neomycin resistance cassette (NeoR, black box) flanked by two FRT sites (yellow triangles). (III) ROSA26 allele after homologous recombination in murine ES cells. **B**, Southern blot analysis of genomic DNA extracted from mouse tail biopsies using 5' probe and 3' probes (indicated in Blue, in A I). The 5' probe detected one gene fragment of 15.6 kb in wildtype (wt), two fragments of 15.6 kb and 8.9 kb in heterozygous (F/+, *R26-lsl-GCaMP3*/wt) and one smaller fragment of 8.9 kb in homozygous mice (F/F, *R26-lsl-GCaMP3/R26-lsl-GCaMP3*). Similarly, the 3' probe detected one gene fragment of 15.6 kb in wildtype, two fragments of 15.6 kb and 11.6 kb in heterozygous, and one smaller fragment of 11.6 kb in homozygous mice. **C**, Coronal brain sections from a P28 *GLAST-CreER;R26-lsl-GCaMP3* mouse that was injected with 2 mg (i.p.) 4-OH-tamoxifen at P14 (P14 + 14). (Left panels) Low magnification images of brain hemisections immunostained for GFP (GCaMP3) and NeuN (neurons) demonstrating widespread expression of GCaMP3. (Middle panels) Images of primary visual cortex (V1) showing $GCaMP3^{+}$ astrocytes in V1 that were $NeuN^{-}$. (Right panels) Images of $GCaMP3^{+}$ $NeuN^{+}$ granule neurons in the dentate gyrus. Images in the left panels were acquired using an epifluorescence microscope, and images in the middle and right panels were acquired using a laser scanning confocal microscope.

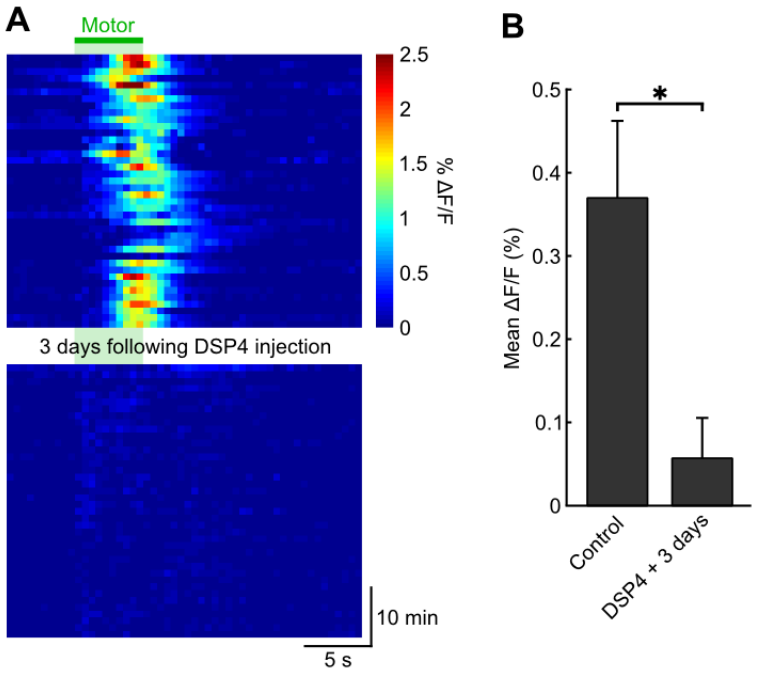

Figure S2 | Chemical disruption of noradrenergic signaling strongly reduces locomotion induced Ca^{2+} elevations in Bergmann glia, related to Figure 2. **A**, Pseudocolored plot of Ca^{2+} elevations (GCaMP3 fluorescence) in Bergmann glia in consecutive trials of enforced locomotion before (top panel) and three days following injection of DSP4 (50 mg/kg i.p.) (lower panel). Green bar highlights period of enforced locomotion. **B**, Summary of population data, bars and symbols represent mean ± SEM (n = 4 mice). Asterisk indicates significant reduction (one-tailed paired t test, p = 0.028).

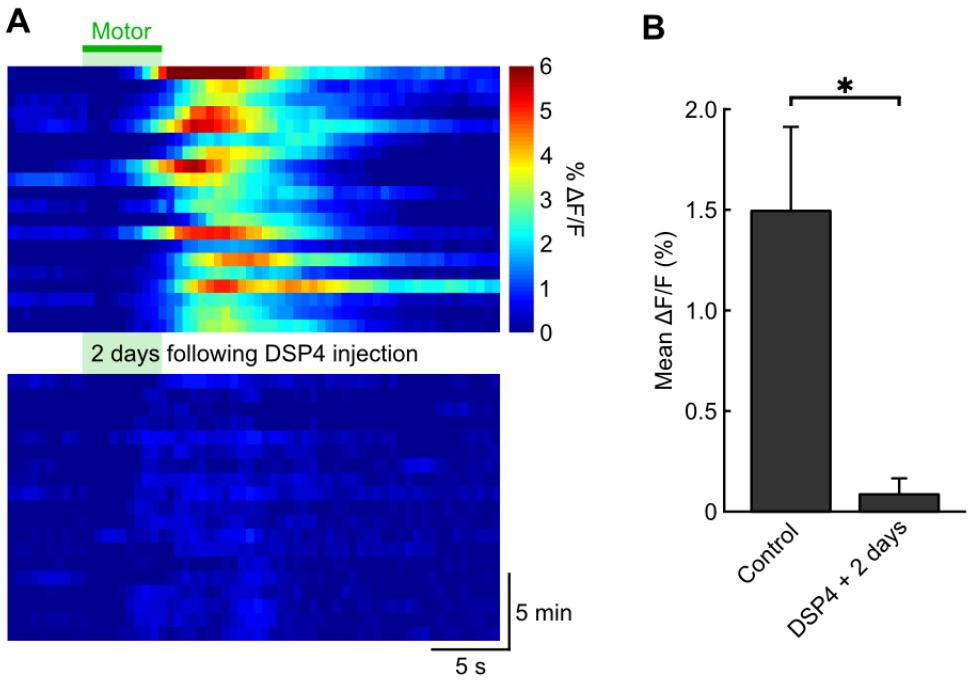

Figure S3 | Chemical disruption of noradrenergic signaling strongly reduces locomotion induced astrocyte Ca^{2+} elevations in primary visual cortex (V1), related to Figure 3. **A**, Pseudocolored plot of Ca^{2+} elevations in V1 astrocytes in consecutive trials of enforced locomotion before (top panel) and two days following injection of DSP4 (50 mg/kg i.p.) (lower panel). Green bar highlights period of enforced locomotion. **B**, Summary of population data, bars and symbols represent mean ± SEM (n = 4 mice). Asterisk indicates significant reduction (one-tailed paired t test, p = 0.030).

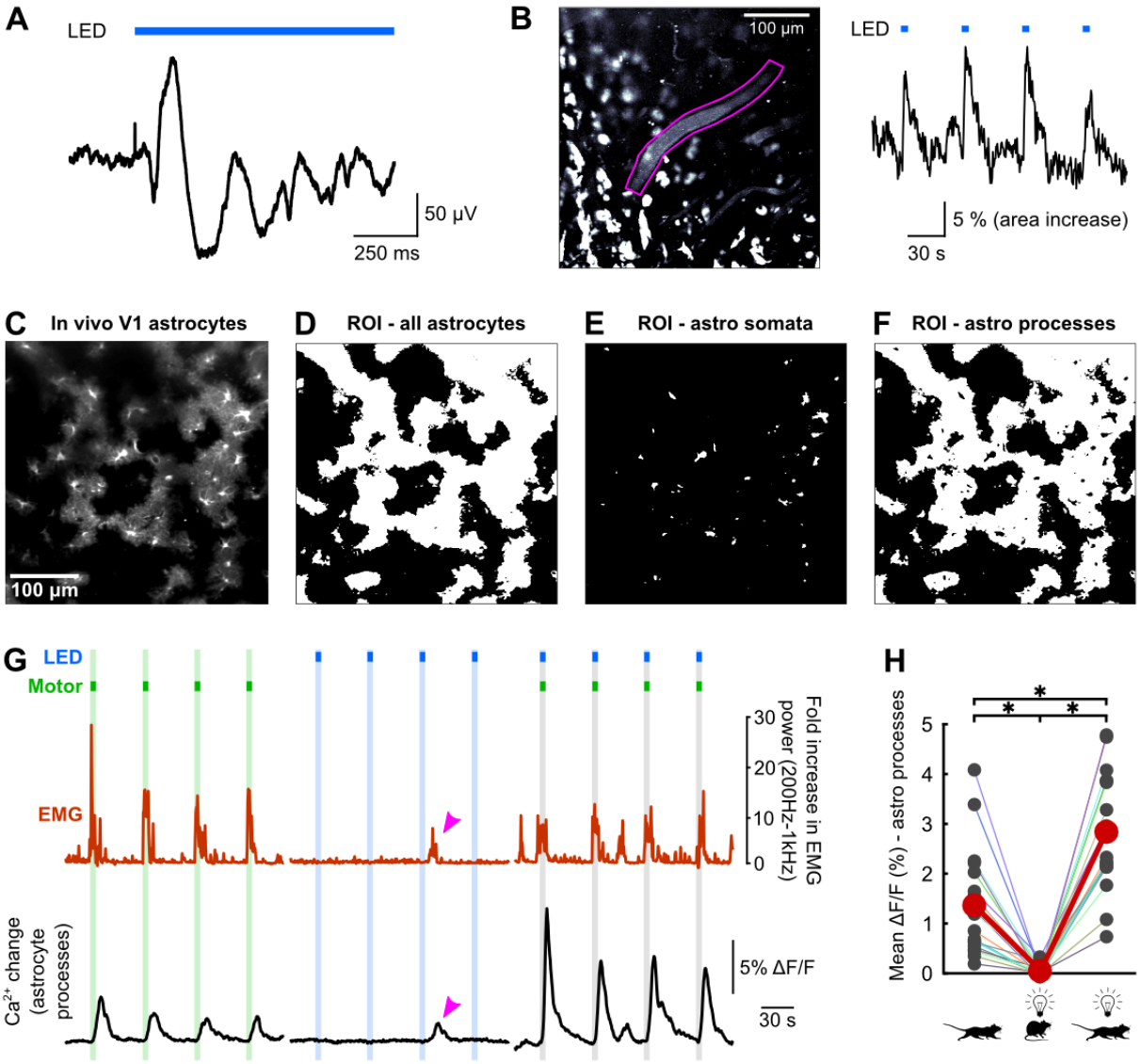

Figure S4 | Norepinephrine enhances the response of astrocyte processes in V1 to light stimulation, related to Figure 4. **A,** Evoked extracellular voltage change (black trace, average of 35 trials) recorded ~150 µm below the pial surface in V1 in response to light exposure for the period indicated by the blue bar. **B,** Left, in vivo fluorescence image of blood vessels filled with dextran-rhodamine labeled plasma in V1. Right, change in area of blood vessel (suprathreshold pixels within highlighted region of interest on the left) induced by light stimulation representing visually evoked hyperemia. Identical intensity and duration of light was used for both measurements and for all light evoked imaging experiments in this study. **C**, In vivo GCaMP3 fluorescence of V1 astrocytes presented in Figure 4A-C. **D**, Region of interest (ROI) map outlining all GCaMP3^{+} astrocytes in the imaging area. **E**, ROI map used to calculate fluorescence changes in astrocyte somata. **F**, ROI map used to calculate fluorescence changes in astrocytes processes (somata blanked). **G**, Plots showing the fluorescence change exhibited by astrocyte processes (black trace) to enforced locomotion alone (green vertical bar), light stimulation alone (blue vertical bar), and simultaneous enforced locomotion and visual stimulation (gray bars). Red traces represent EMG activity. Arrowheads highlight a Ca^{2+} elevation and EMG activity associated with spontaneous locomotion. **H**, Graph of the mean change in GCaMP3 fluorescence for all astrocyte processes in each condition (16 - 20 trials). Colored lines connect data points from individual mice. Asterisks indicate significant difference (one-way ANOVA with Bonferroni post-hoc test). Red circles represent the mean of all trials.

Movie S1 | Series of *in vivo* two-photon images through the cerebellar cortex of an adult *GLAST-CreER;R26-lsl-tdtomato* mouse, related to Figure 1. Left, singIe optical section. Right, white bar within side view highlights imaging depth of single optical section on left. Imaged volume was 250 µm x 250 µm x 250 µm. Step size in z-direction was 2 µm; for display purposes side view image was oversampled in z-direction 8-fold followed by interpolation.

Movie S2 | Locomotion induced Ca^{2+} elevations in cerebellar Bergmann glia, related to Figures 1 and 2. *In vivo* two-photon imaging time series. Optical section 70 µm below pial surface through the cerebellar molecular layer of an adult *GLAST-CreER;R26-lsl-GCaMP3* mouse. Imaging area: 400 µm x 400 µm. Video was accelerated 2-fold. Green bar indicates average locomotion speed during displayed image frame.

Movie S3 | Locomotion induced Ca^{2+} elevations in visual cortex astrocytes, related to Figure 3. *In vivo* two-photon imaging time series. Optical section 60 µm below pial surface through primary visual cortex (V1) of adult *GLAST-CreER;R26-lsl-GCaMP3* mouse. Imaging area: 400 µm x 400 µm. Video was accelerated 2-fold. Red bar indicates average increase in EMG activity compared to rest and green bar indicates average locomotion speed during displayed image frame.

SUPPLEMENTAL EXPERIMENTAL PROCEDURES

All procedures were approved by Johns Hopkins University Animal Care and Use Committee.

Animals. *Gene Targeting in Embryonic Stem Cells and Generation of R26-lsl-GCaMP3 Knock-In mice.* Conditional GCaMP3 mice were generated using a knock-in strategy into the ROSA26 locus. For inducible expression of GCaMP3, we incorporated a transcriptional "stop" sequence (3x SV40 polyA) flanked by loxP sites (loxP-stop-loxP, LSL); the presence of the stop sequence prevents expression of GCaMP3 until Cre recombinase excises this DNA. To have ubiquitous and robust expression, we engineered GCaMP3 under control of the CAG promoter, a chicken β-actin promoter with a 5' cytomegalovirus early enhancer element, and as a 3' UTR we incorporated WPRE (woodchuck hepatitis virus posttranscriptional regulatory element) sequence. WPRE leads to the early exit of mRNA from the nucleus as well as enhances the stability of mRNA in the cytosol. The final GCaMP3 targeting vector (pAA004) was assembled by cloning *CAG-LSL-GCaMP3-WPRE* gene fragment into a ROSA26 targeting plasmid (obtained from Dr. Jeremy Nathans at Johns Hopkins University) containing 2.2 kb 5' homology arm, 4.3 kb 3' homology arm, PGK-Neomycin resistance cassette (immediately upstream of 3' homology arm) for positive selection and PGK-DTA (downstream of 3' homology arm) for negative selection. The embryonic stem (ES) cells derived from a SV129 mouse strain were electroporated with the *AsiSI* linearized targeting vector pAA004. A nested PCR screening strategy along the 5' homology arm was used to identify ES cell clones harbouring the correct genomic targeting event. To confirm the proper targeting, southern blot analysis was performed on *EcoRI* digested genomic DNA isolated from PCR positive ES cell clones and probed with a 494 bp long P^{32}-labeled probe located 123 bp upstream 5' homology arm of ROSA26 gene. In order to confirm the integrity of targeted ROSA26 locus, *EcoRI* digested ES cell genomic DNA was probed with P^{32}-labeled 375 bp probe located 2.9 kb downstream of 3' homology arm of ROSA26. After confirmation of the karyotypes, two correctly targeted ES cell clones were used to generate chimeric mice by injection into blastocysts derived from SV129 females at the Johns Hopkins University Transgenic Core Laboratory. Germ line transmission was achieved by breeding male chimeric founders to C57Bl/6N wild-type female mice. Routine genotyping of *R26-lsl-GCaMP3* mice was performed by PCR using primers following primers: R26U1 (ROSA26-s, 5'-ctctgctgcctcctggcttct-3'), R26U2 (ROSA26-as, 5'-cgaggcggatcacaagcaata-3') and R26U3 (CMV-enhancer-as, 5' tcaatgggcgggggtcgtt-3'). These primers will amplify a 327bp DNA fragment for the wildtype ROSA26 allele, 247 and 327 bp fragments for heterozygous GCaMP3 mice, and a single 247 bp fragment for homozygous GCaMP3 mice. The presence of the Neomycin resistance cassette did not have any adverse effects on the expression of GCaMP3 or the health and survival of *R26-lsl-GCaMP3* mice. Hence, in the current study our mice still harbour the flipped PGK-Neomycin resistance gene. This cassette can be removed by crossing GCaMP3 heterozygous mice to FLP deleter mice. *GLAST-CreER;R26-lsl-GCaMP3* mice were injected with 3 x 100 mg/kg body weight of tamoxifen i.p. at 48 hour intervals at P21-P30, surgery was performed on 4-5 week old animals and imaging sessions were begun at least two weeks later. For routine imaging, 35 µl of 3% dextran-rhodamine (MW 70,000) in saline was injected into one of the saphenous veins.

Animal surgery. Craniotomies were performed in two steps. In the first surgery, a custom designed stainless steel plate was attached to the skull for immobilization of the head under the objective. In the second surgery, performed at least 3 days later, the bone was removed and replaced with a coverslip. Mice were anaesthetized by i.p. injection of ketamine (100 mg/kg) and xylazine (10 mg/kg). As soon

as animals were unconscious, petroleum jelly was applied to the eyes. The scalp was incised, resected, and a mixture of lidocaine HCl and epinephrine (Hospira; 10 mg/ml and 10µg/ml, respectively) were applied topically before the skull was exposed. For surgeries on the cerebellum, superficial neck muscles were resected to expose the skull above vermis and left hemisphere. For all surgeries, the periostium was then shaved off and approximately 3 mm of muscle surrounding the exposed skull was covered with a thin layer of cyanoacrylate cement. After drying, an 11 mm wide aluminum head plate with a 4 mm x 6 mm oval opening was centered above crus II / paramedian lobule of the cerebellar hemisphere (Figures 1, 2; Figure S2), above primary visual cortex V1 at lambda, 2.5 mm lateral from midline (Figures 3, 4; Figures S3, S4) or above transverse sinus between V1 and lobulus simplex (Figure 3F-H), and attached to the skull using dental cement (C&B Metabond; Parkell Bio-Materials Div.). The second surgery was performed at least three days (at least one week for acute imaging experiments; Figure 2G) after mounting of the head plate under ketamine / xylazine anaesthesia (under 1.5-2 % vol./vol. isoflurane in O_2 for acute imaging experiments). A 2.5 mm x 2.5 mm (2.5 mm x 5 mm for Figure 3F-H) area of skull in the center of the opening was removed using a scalpel blade #12. A No.1 cover glass was placed on the dura mater and the edges sealed with dental cement (Caulk Division, Dentsply International; Grip Cement). Imaging was initiated at least two weeks after surgery. The time during recovery from the second surgery, or between first and second surgery for acute imaging experiments, was used to habituate the mouse to the linear treadmill and the imaging environment.

***In vivo* two photon imaging.** Fluorescence images were collected using a Movable Objective Microscope (MOM) (Sutter Instrument) with a Zeiss 20x, 1.0 NA objective. The microscope was controlled by a personal computer equipped with an Intel Core i7 CPU 950 @ 3.07 GHz and 3 GB of RAM running ScanImage (v3.6) software (Pologruto et al., 2003) and custom scripts modified from TrImager software (Paukert and Bergles, 2012). Acquired frames were 400 µm by 400 µm at 512 by 512 pixel resolution. Image acquisition rate was 2 frames/s. Two photon excitation was achieved using a Titanium:Sapphire laser (Chameleon Ultra II, Coherent) tuned to 900 nm and attenuated, so that an average power of 45 mW or less entered the brain. The head of the mouse was immobilized by attaching the head plate to a custom machined stage mounted on the microscope table. Mice were kept on the stage for a maximum of two hours.

Dual optic fiber bundle imaging. For simultaneous single photon fiber optical imaging of cerebellum and visual cortex, the optical axes of the two fiber bundles at the animal's ending were arranged with a separation of 3.5 mm. The excitation light from the fiber bundles was focused into the tissue and the emitted light was collected through coupling / objective lenses placed in close proximity to the cover glass of the cranial windows (see schematic in Figure 3F). The following parts were used for the microscope: 488 nm laser, OBIS488LS 20 mW, Coherent; 10x beam expander, BE10M-A, Thorlabs; dichroic mirror, FF499-Di01-25x36, Semrock; objective lens, Plan 4x/0.10 NA Olympus; fiber bundles with 650 µm diameter - 600 µm diameter field of view, FIGH-30-650S, Fujikura; coupling/objective lens, aspheric lens pair, 352140-A/0.55NA, Thorlabs; GFP emission filter; focusing lens, achromatic doublet lens, AC254-150-ML-A, Thorlabs; CCD camera, GS2-FW-14S5M, Point Grey Research. Optical cross-talk between the fiber bundles was minimal: The coupling / objective lens pairs had a diameter of 2.4 mm and a working distance of 0.88 mm. Thus, with a distance of 3.5 mm separating the optical axes of the two fiber bundles, capturing light from the other structure would be very inefficient. If such cross-talk occurred and Ca^{2+} responses in cerebellum and visual cortex did

not co-vary, we would expect many instances of small responses in one probe accompanying robust responses in the other; however, the majority of responses were of similar size (Figure 3H). In addition, if cross-talk between fibers was the cause of co-variation, responses measured by the two fibers should have the same kinetics; however, while the onset of the two signals was not significantly different, the signal from visual cortex reached its peak significantly later than the signal from cerebellum.

Locomotion behavioral paradigm. Head immobilized mice were placed on a custom designed linear treadmill. The treadmill was either freely movable so that animals could move at will, or it was under motor control. The motion of the belt of the treadmill was monitored with a mechanically coupled optical encoder. The signal of the optical encoder was digitized at 20 kHz simultaneously with the mirror position signal of the slow scan galvanometer (Digidata 1440A, Molecular Devices) for post hoc determination of movement velocity during corresponding images.

Electromyography. Body surface potentials were recorded as the voltage difference between two silver wires placed subcutaneously at the right shoulder and left hip using an electrocardiogram amplifier (Sigmann Elektronik) and an instrumentation amplifier (Brownlee Precision; Model 440). Data were digitized at 20 kHz (Digidata 1440A, Molecular Devices) for post hoc analysis. Muscle activity was extracted by applying a fast Fourier transform to the data and determining the power in the range 200 Hz - 1 kHz. Fold increase was determined as power / $power_{Baseline}$.

Visual stimulation. A UV-LED (UVTOP-355-TO39-FW, Sensor Electronic Technology Inc.) with a Lambertian emission profile was used as a light source at a distance of 40 mm centered between the eyes to achieve uniform light exposure. The light power entering each eye with a pupil diameter of 2 mm was 7 nW. To eliminate optical cross talk between visual stimulation and two-photon fluorescence detection, the objective was shielded from the light source.

Visual evoked potential recordings. A 3 mm x 3 mm area of bone covering primary visual cortex was removed under isoflurane anaesthesia (1.5-2 % vol./vol. in O_2) from 4 week-old *GLAST-CreER;R26-lsl-GCaMP3* mice, as described above. The brain was covered with artificial cerebrospinal fluid (ACSF), containing in mM: 137 Na^+Cl^-, 2.5 K^+Cl^-, 1 $Mg^{2+}Cl^-_2$, 2 $Ca^{2+}Cl^-_2$, 20 Hepes, pH adjusted to 7.3 using NaOH. The tip of a glass micropipette filled with ACSF and a tip resistance of 6 MΩ was placed 150 µm below the pial surface. The reference electrode was placed on the surface of the bone covering the rostral forebrain and submersed in ACSF solution. The potential difference was recorded in current-clamp mode using a Multiclamp 700B amplifier (Molecular Devices) and recordings were filtered at 5 kHz and digitized at 20 kHz (Digidata 1440A, Molecular Devices). Visual stimulation episodes lasting 5 s were delivered once per minute.

Pharmacology. *Systemic:* Mice were exposed to the following dosages of solvents for i.p. injection of lipophilic drugs (µl/10g body weight): trazodone: 3 DMSO + 3 Tween 80; metergoline: 5 DMSO + 5 Tween 80; 2-Methyl-6-(phenylethynyl)pyridine (MPEP): 18 DMSO; AM251: 3 DMSO + 6 Tween 80. *Acute* (Figure 3G): In order to optimize access of drugs to the cerebellum while preserving integrity of the tissue we removed the dura following removal of the skull and continuously superfused the surface of the cerebellum with ACSF. In order to dampen tissue movement associated with the mouse walking on the treadmill we cemented (Caulk Division, Dentsply International; Grip Cement) a

3 mm (rostrocaudal direction) by 800 μm strip of No. 1 cover glass across the skull window. The center 2 mm of the glass strip was extended by gluing an additional 2 mm by 800 μm strip of No. 1 cover glass to it using a UV curable optical adhesive (Norland Optical Adhesive 61, Norland). This procedure provided sufficient gentle pressure against the surface of the cerebellum to enable two-photon imaging during locomotion events while providing access for diffusion of drugs into the underlying tissue that was imaged.

Immunocytochemistry. Mice were perfused by cardiac puncture with 4% paraformaldehyde in phosphate buffer (PB). Brains were then removed and immersed in the same fixative for 4 h at 4°C. Free-floating parasagittal sections (35 μm) were prepared using a Vibratome (VT1000S, Leica) and collected in PB. Sections were rinsed, blocked against nonspecific antibody binding, and permeabilized in PB containing 5% normal donkey serum (NDS) and 1% Triton X-100 for 3 h. Sections were then incubated for 36 h at 4°C in PB containing 5% NDS, 0.5% Triton X-100, primary antibodies, rabbit α-GFAP (1:500, Millipore) and guinea pig α-GFP (1:500, gift from M. Fukaya) (Figure 1A), and rabbit α-GFAP (1:500, Millipore) and goat α-GFP (1:200, SICGEN) (Figure 3A, B and Figure S1). After rinsing, sections were incubated for 3 h at room temperature in PB containing 5% NDS and Cy2- and Cy5-conjugated secondary antibodies against guinea pig or goat and against rabbit (1:1000; Jackson ImmunoResearch), respectively. Images in Figures 1A and 3B were obtained using a Zeiss LSM 510 confocal microscope with a Zeiss 40x oil immersion, 1.3 NA objective and the pinhole set to less than 1 airy unit. Images represent maximum intensity projections of image stacks with a step size of 0.5 μm covering 8-10 μm. Figure 1A represents a tiled image. The image in Figure 3A was taken at a Zeiss AX10 Imager M1 microscope using a Zeiss 2.5x, 0.12 NA objective.

Data Analysis. Data were processed and analyzed in MATLAB using built-in functions integrated into custom routines. Images were first processed with a Gaussian filter (1.52 SD per pixel distance) to reduce stochastic noise of the detector. To compensate for motion artifacts during image series, a whole-frame normalized 2D cross-correlation (built-in function “normxcorr2”) was determined for dextran-rhodamine images, and individual frames were registered to maximize correlation. The same registration parameters were then applied to images of GCaMP3 fluorescence. ΔF/F fluorescence intensity ("Ca^{2+} change") traces represent $(F - F_{median}) / F_{median}$ with F representing mean fluorescence value of all pixels within a region of interest (ROI) of one image frame and F_{median} representing median F of all image frames. ROIs were the entire image frame (Figures 1, 2 and Figure S2), thresholded area distinguishing GCaMP3 expressing astrocytes from background (Figures 3C-E, 4A and D, Figure S3), individual astrocytes (Figure 4A-C) or area representing each fiber bundle (Figure 3F-H). Quantification of individual Ca^{2+} responses represents the peak (Figures 1E, 3H) or mean ΔF/F within 0 -10 s (cerebellum) or 2.5 - 12.5 s (visual cortex) following the onset of locomotion or stimulation. For the analysis of astrocyte responses to light stimulation alone in Figure 4D, we analyzed trials in which during the episode from 2 s preceding light stimulation until 2 s following light stimulation the EMG signal never exceeded 2.2 fold relative to baseline. This criterion was chosen to exclude trials during which the mouse voluntarily engaged in locomotion or showed a startle response. For analysis of the correlation between the magnitude of the Bergmann glia Ca^{2+} change and locomotion speed (Figure 1E), we used the following statistical strategy to identify response failures to locomotion (which were excluded from the correlation analysis): we determined the mean and standard deviation (SD) of 15 consecutive ΔF/F values preceding the onset of locomotion (baseline). If the difference between the mean of the 10 largest ΔF/F values within 15 consecutive ΔF/F values from onset of

locomotion and the mean of the baseline did not exceed 2 * SD of the baseline, it was considered a failure.

Statistical Analysis. Figures 1E and 3H: analysis of co-variance for correlation within subjects (Bland and Altman, 1995); Figures 1B and C, 4D (right), difference in onset of response in Figure 3F-H, Figures S2 and S3, one-tailed paired *t* test; Figures 1F and G, 4C and D (left) one-way ANOVA followed by Bonferroni post-hoc test; text, difference in peak of response in Figure 3F-H, one-sample *t* test.

References

Bland, J.M. and Altman, D.G. (1995). Calculating correlation coefficients with repeated observations: Part 1 - correlation within subjects. BMJ *310*, 446.

Paukert, M. and Bergles, D.E. (2012). Reduction of motion artifacts during in vivo two-photon imaging of brain through heartbeat triggered scanning. J. Physiol. *590*, 2955-2963.

Pologruto, T.A., Sabatini, B.L., and Svoboda, K. (2003). ScanImage: flexible software for operating laser scanning microscopes. Biomed. Eng. Online *2*, 13.